Discrete Molecular Dynamics Study of $A\beta$16-22 Folding and Aggregation

S. Peng[†,*], B. Urbanc[†], S. V. Buldyrev[‡], L. Cruz[†], S. Yun[†],

D. B. Teplow[♮] and H. E. Stanley[†]

September 21, 2005

[†]Center for Polymer Studies and Department of Physics,

Boston University, Boston, MA 02215;

[‡]Department of Physics, Yeshiva University, New York, NY 10033,

[♮] Department of Neurology, David Geffen School of Medicine,

University of California, Los Angeles, CA 90095.

[*]Corresponding author. Email: shypeng@bu.edu

ABSTRACT

Alzheimer's disease (AD) is the most common cause of late life dementia. Substantial clinical and experimental evidence supports the hypothesis that amyloid β-protein ($A\beta$) aggregation produces assemblies with potent neurotoxic properties that cause AD. For this reason, it is important to elucidate the structural dynamics of $A\beta$ aggregation at atomic level. We apply the discrete molecular dynamics method coupled with a four-bead protein model to study the aggregation of $A\beta$16-22, a peptide that contains the $A\beta$ central hydrophobic cluster, Leu_{17}–Ala_{21}, found to be crucial in mediating $A\beta$ assembly. Backbone hydrogen bond interactions are incorporated into the model. Effective hydrophobic and electrostatic interactions between side-chains are parameterized using amino acid-specific hydropathies and net charges. The aggregation of up to 16 $A\beta$16-22 peptides is studied. The results show that randomly-oriented monomers can aggregate into fibrillar subunits. These subunits consist of multi-layer β-sheets that resemble the well-known cross-β structure as revealed by X-ray diffraction studies of amyloid fibrils. An antiparallel arrangement of β-strands is observed within each β-sheet, which agrees with solid-state NMR studies. In the absence of electrostatic interactions the peptides aggregate into amorphous (disordered) structure,

suggesting that the electrostatic interactions are crucial to the antiparallel β-sheet organization. Heat capacity calculations show that $A\beta$16-22 assembly and melting are two-stage processes, a prediction that can be tested experimentally using differential scanning calorimetry. Continued investigation of intermediate assembly states along the fibril formation pathway promises to reveal mechanistic features of $A\beta$ assembly of value in the design of therapeutic agents.

Keywords: Alzheimer's disease, amyloid β-protein, discrete molecular dynamics simulations, cross-β structure

1 Introduction

Neurodegenerative diseases such as Alzheimer's disease (AD), Parkinson's disease, and prion diseases share certain features, including protein misfolding and aggregation (Taylor et al., 2002). AD is the most prevalent among these diseases and is also the most common cause of late life dementia (Selkoe, 1991). According to the amyloid cascade hypothesis (Hardy and Selkoe, 2002), AD results from the aberrant assembly of the amyloid β-protein ($A\beta$), leading to direct peptide-mediated neurotoxic effects as well as a cascade of associated injurious physiologic events. The first assembly process recognized in AD was amyloid formation (Alzheimer, 1906), which leads to the accumulation of senile plaques in the brains of AD patients (Selkoe, 2001). Plaques comprise dense deposits of insoluble $A\beta$, organized into stable fibrils, and numerous other proteins and macromolecules. Therapeutic efforts over the last century have focused on fibril elimination and prevention. Recent studies of fibril formation have revealed an increasing number of pre-fibrillar, oligomeric assemblies that are potent neurotoxins and may be the proximate effectors of AD neuropathology (Lambert et al., 1998; Walsh et al., 1999; Klein et al., 2001, 2004; Hardy and Selkoe, 2002; Kirkitadze et al., 2002). In fact, senile plaque formation may be an end-stage event in AD, or even

protective (Roher et al., 2000; Rottkamp et al., 2002). To understand the toxicity of pre-fibrillar assemblies, and to prevent the formation of toxic intermediates, it is important to determine not only their structures but also their assembly mechanisms at atomic level.

Traditional all-atom molecular dynamics (MD) simulations using realistic force fields in physiological solutions require immense computational power and are thus currently limited to time scales insufficient to study $A\beta$ aggregation. However, coarse-grained protein models with simplified interactions can accelerate simulations of protein folding and aggregation without losing the ability to reveal key mechanistic features of the process (Shakhnovich, 1996). Coarse-grained protein models with discrete molecular dynamics (DMD) algorithms have been applied in the study of protein folding and aggregation (Zhou and Karplus, 1997; Dokholyan et al., 1998; Zhou and Karplus, 1999; Smith and Hall, 2001a,b; Nguyen and Hall, 2004b,a, 2005; Borreguero et al., 2002; Ding et al., 2002a,b, 2003; Peng et al., 2004; Urbanc et al., 2004a,b; Borreguero et al., 2005; Ding et al., 2005). A two-bead protein model has been applied to the study of the Src SH3 domain (Ding et al., 2002a,b), c-Crk SH3 domain (Borreguero et al., 2002), and $A\beta$1-40 peptide (Peng et al., 2004). A four-bead protein model has been applied to the

study of polyalanine (Ding et al., 2003) and $A\beta$1-40 and $A\beta$1-42 peptides (Urbanc et al., 2004a,b). A coarse-grained protein model with more side-chain details has been applied to the study of Trp-cage (Ding et al., 2005). A united-atom model, where all the atoms except hydrogens are modeled explicitly, has been applied to study folding events of $A\beta$21-30 (Borreguero et al., 2005).

$A\beta$16-22 is an attractive $A\beta$ fragment to study $A\beta$ folding and assembly because (i) it is one of the shortest $A\beta$ fragments that forms fibrils *in vitro* and (ii) it contains the central hydrophobic cluster, Leu_{17}–Ala_{21}, that plays an important role in the fibril formation of full-length $A\beta$ (Esler et al., 1996; Lynn and Meredith, 2000). $A\beta$16-22 has been studied by experimentalists (Balbach et al., 2000; Petkova et al., 2004) and theoreticians (Ma and Nussinov, 2002; Klimov and Thirumalai, 2003; Klimov et al., 2004; Hwang et al., 2004; Favrin et al., 2004; Santini et al., 2004a,b). Solid-state NMR reveals that $A\beta$16-22 forms well-ordered, antiparallel fibrils under physiological conditions (Balbach et al., 2000; Petkova et al., 2004). All-atom molecular dynamics simulations, which have been used to test the stabilities of structural models based on experimental results (Ma and Nussinov, 2002), would be an ideal tool for illustrating how monomers aggregate into extended β-sheets

comprising fibrils, but they are limited by current computational power to a small number of $A\beta$16-22 peptides (Klimov and Thirumalai, 2003; Klimov et al., 2004; Hwang et al., 2004) and other small peptides (Gsponer et al., 2003; Paci et al., 2004; Wei et al., 2004).

Here we study $A\beta$16-22 folding and aggregation of 8 and 16 $A\beta$16-22 peptides using the DMD method combined with a four-bead protein model (Ding et al., 2003). In this model, each amino acid is represented by up to four "beads", with three beads representing the protein backbone and the fourth bead representing the amino acid side-chain. The amino acids interact through backbone hydrogen bond interactions (Ding et al., 2003) as well as amino acid-specific effective hydrophobic and electrostatic interactions between side-chains (Urbanc et al., 2004b). The temperature is controlled by a Berendsen thermostat (Berendsen et al., 1984). Our results show that randomly-oriented $A\beta$16-22 monomer peptides aggregate into β-sheet structures, in which neighboring peptides have antiparallel orientations and the β-sheets are stacked into multiple layers. This organization is consistent with experimentally determined structures (Balbach et al., 2000). In addition, the computed X-ray diffraction pattern of our simulated multi-layer β-sheet assemblies is qualitatively consistent with experimental observations (Malinchik

et al., 1998; Serpell, 2000). The well-ordered free edges (Richardson and Richardson, 2002) of these structures may enable further fibril extension reactions. Our results also show that aggregation is a "two stage" process. The initial globular hydrophobic collapse into an amorphous (disordered) structure is followed by "one-by-one" hydrogen bond formation, leading into an ordered antiparallel β-sheet structure. In the absence of the electrostatic interactions the peptides aggregate into amorphous structures, which testifies that the electrostatic interactions are crucial to the ordered antiparallel β-sheet structure in agreement with Klimov and Thirumalai (2003).

2 Methods

2.1 Discrete molecular dynamics

When all interactions between particles in a system are simplified to square-well potentials or their combinations, a DMD algorithm can be applied to simulate the dynamics of the system. In DMD, each particle in the system only experiences "collisions" (elastic or/and inelastic) at distances where their interaction potential changes. Between consecutive collisions at times t_i and t_{i+1}, all particles move along straight lines with constant velocities.

The DMD simulation keeps track of the state for each particle and maintains a set of all possible collisions, collision table, and then sorts out the pair of particles with the shortest collision time. If the particles p and q collide at the time t_{i+1}, the states of the two particles will be updated according to the laws of both energy and momentum conservations, and the time will be set to t_{i+1}. Then all the outdated collision events related to p and q will be updated for calculating the new possible collisions related to p or q. These new possible collisions will be inserted into the collision table to find the next collision event. Therefore, at each collision event, only the involved pairs of particles need to be updated to keep track of their new states and the rest of the system remains intact.

The DMD algorithm is the following:

1. Initialize the system, construct the table of all possible collisions;

2. Sort out the earliest collision event, and identify the particles p and q involved in the collision;

3. Update the state of the particles p and q according to the laws of conservation of energy and momenta;

4. Update the collision table by considering all possible collisions with the

particles p and q;

5. Repeat the steps 2,3,4.

The speed of the most efficient DMD algorithm is proportional to $N \ln N$, where N is the total number of atoms (Rapaport, 1997), and the speed of the algorithm decreases linearly with the number of square-well discontinuities in the potential and the particle density. Combined with a coarse-grained protein model, the DMD algorithm is computationally more efficient compared to the traditional all-atom MD method because: (1) positions and velocities are updated only for particles experiencing collisions; (2) solvent is not explicitly present, which significantly reduces the number of particles in the system; and (3) the number of particles in the peptide is reduced further through coarse-graining.

We perform DMD simulations in the canonical ensemble (NVT). We use the Berendsen thermostat algorithm (Berendsen et al., 1984) to maintain the temperature of the system. This is done through coupling the system to an external bath. Assuming that the initial temperature of the system is T_i, the final temperature (i.e. the temperature of the heat bath) is T_f, and the heat exchange rate is α ($\alpha = 0.01$ in our simulations). If we "update" the

temperature at a regular small time interval δt,

$$T(t+\delta t) - T(t) = [T_f - T(t)]\alpha\delta t\,, \tag{1}$$

the system will approach the final temperature exponentially:

$$T(t) = T_f + (T_i - T_f)\exp(-\alpha t)\,. \tag{2}$$

The temperature T of a system is defined by the kinetic energy of the system,

$$\frac{3}{2}k_B T \equiv \frac{1}{N}\sum_{i=1}^{N}\frac{mv_i^2}{2}\,, \tag{3}$$

where N is number of particles in the system.

2.2 Four-bead model and interactions

Four-bead models have been applied to the study of the folding of a designed three-helix-bundle protein (Takada et al., 1999), the assembly of a tetrameric α-helical bundle (Smith and Hall, 2001a,b), and the aggregation of polyananines (Nguyen and Hall, 2004a,b, 2005). The four-bead model used in this study predicts an α-helix$\rightarrow\beta$-hairpin transition (Ding et al., 2003), an important step in fibril formation. In recent studies of $A\beta$ dimer formation, this model predicted several β-strand-rich planar dimer conformations (Urbanc et al., 2004a). The four-bead model with amino acid-specific interactions due

to hydropathy captures general features of the observed *in vitro* oligomerization differences between the two predominant full-length forms of $A\beta$ found *in vivo*, $A\beta$1-40 and $A\beta$1-42 (Urbanc et al., 2004b).

2.2.1 Geometry of the model protein

In the four-bead model, each amino acid in a protein is modeled by four beads (Ding et al., 2003)—one bead each for the α-carbon, C_α; the amide nitrogen, N; the carbonyl group C'; and the side-chain atoms, C_β. The exception is Gly, which lacks C_β.

2.2.2 Interactions

A backbone hydrogen bond interaction is introduced between the C' bead of one and the N bead of another amino acid. Because a hydrogen bond is directional, auxiliary bonds are introduced to model the angular dependence of the hydrogen bond as described in detail elsewhere (Ding et al., 2003). The strength of the hydrogen bond interaction is ϵ_{HB}.

Effective hydrophobic interactions between pairs of hydrophobic amino acids are introduced to simulate the solvent effect (Urbanc et al., 2004b). They are modeled by a single attractive potential well with an interaction

range from 3.07Å to 7.5Å (shown in Fig. 1 (a)). Interaction strengths are determined by the average hydrophobicity of the two amino acids involved. The hydrophobicities for hydrophobic amino acids are rescaled to [0,1] based on the Kyte-Doolittle (1982) hydropathy scale with Ile as the most hydrophobic amino acid with a hydrophobicity 1.0, followed by Val (0.93), Leu (0.84), Phe (0.62), Met (0.42), and Ala (0.40).

In addition to the effective hydrophobic interactions, we introduce effective electrostatic interactions between two charged amino acids. Because of the "screening" effect of polar water molecules, the effective electrostatic interaction is much weaker than in vacuum, and approximated by a "short-range" interaction. We use a cutoff distance 7.5Å and model it by a double-well potential (shown in Fig. 1 (b)). The interaction between two oppositely-charged amino acids is modeled by an attractive double-well potential, whereas the interaction between two identically-charged amino acids is modeled by a repulsive double-well potential. Charged amino acids interact with hydrophobic amino acids only through hard-core repulsion.

2.3 Energy and Time Units

The strength of the hydrogen bond interaction, ϵ_{HB}, is the energy unit, the mass of a carbon atom, m_c, is the unit of mass, and $l_0 \equiv 1\text{Å}$ is the unit of length in our simulations. The time unit is $l_0\sqrt{m_c/\epsilon_{HB}}$. Due to the absence of solvent molecules, the kinetics is not well represented in DMD. Thus, the simulation time can not be directly related to the real time. However, the thermodynamics as well as the temporal sequence of events should remain intact.

2.4 Limitations

The peptide model parameters (the peptide bonds and constraints) and the parameters of the hydrogen bonding, are defined phenomenologically using the known crystalline structure of proteins from the Protein Data Bank (PDB). These parameters might depend on the particular protein database. However, for our purposes the peptide model parameters are fixed and represent the definition of the peptide model.

We approximate each side-chain (except Gly) by one atom. This model thus neglects the size differences and geometrical details of each side-chain. Instead, the specificity is introduced only through the amino acid specific

interactions with individual hydropathies and charge. This approach follows the assumption that the sequence of hydrophobic/hydrophilic amino acid essentially drive folding and aggregation (Xiong et al., 1995).

All interactions are modeled by a square-well or a combination of square-well potentials. That is a particularly crude approximation for an electrostatic interaction, which is by nature long-range (Rapaport, 1997). However, in an aqueous solution there is always shielding of charged atoms (by polar solvent molecules), rendering the electrostatic interactions effectively short-range, which makes a double square-well potential approximation in our approach more plausible.

Hydrogen bond, effective hydrophobic/hydrophilic, and electrostatic interactions depend on the particular solvent surrounding the peptides. We can adjust the hydrogen bond, hydropathic, and electrostatic interaction potential energies accordingly. In aqueous solutions hydrogen bond, hydropathic, and electrostatic interactions depend strongly on the exposure of individual peptide groups to water molecules. The hydrogen bond interaction is stronger within the protein core where there's no water molecules than at the surface of the protein where the protein can form hydrogen bonds with water molecules. The effective hydropathic interaction, on the other hand, is

stronger at the surface and weaker within the protein core where there's no contacts with water molecules. Similarly, the free energy change associated with breaking a salt-bridge within the hydrophobic core of a protein is much higher than at its surface, where polar water molecules shield the charged atoms and thus effectively weaken the electrostatic interactions between the side-chains. Our DMD approach does not incorporate these local effects into inter-particle interactions.

Despite these limitations, the DMD approach is one of few that permits to study assembly of many peptides simultaneously, track evolution of intra- and inter-particle contacts and structure during oligomer and/or fibril formation, and obtain statistically significant results.

3 Simulation Results

It has been shown that the four-bead $A\beta$ model, which is essentially a polyalanine chain with glycines at positions 9, 25, 29, 33, 37, and 38, and which incorporates hydrogen-bonding but no amino acid-specific interactions, predicts a β-hairpin monomer conformation with a turn centered at Gly25-Ser26 and planar β-strand dimer conformations (Urbanc et al., 2004a). The same

model, with amino acid-specific interactions due to hydropathy ($\epsilon_{HP} = 0.3$), produces globular oligomers with hydrophobic residues at the core and hydrophilic residues at the surface of the oligomer (Urbanc et al., 2004b). A similar polyalanine model without glycines and with a relatively weaker hydrophobic interaction ($\epsilon_{HP} = 1/8$) produced parallel β-sheets (Nguyen and Hall, 2004a). The effects of hydrophobic interactions on peptide folding have been studied by Ding et al. (2003) who did simulations of 16 amino acid long polyalanine using the four-bead model with variable ratios of $\rho = \epsilon_{HP}/\epsilon_{HB}$ (0.05, 0.10, 0.15, ..., 0.50) and found that the β-hairpin state becomes less stable with increasing ρ. For small ρ, the thermodynamic property of this polyalanine resembles that of the peptide without hydrophobic interactions. At a characteristic range of values [0.20 0.35], the intermediate β-hairpin state disappears and the peptide folds cooperatively into the native α-helix state. At large ρ, peptide can only fold to a molten globular state. Therefore, $\rho < 0.20$ would allow for the ordered hydrogen bonded structures. In the present study the maximum hydrophobic interaction strength, ϵ_{HP}, which occurs between two isoleucines, is set to 0.15 relative to ϵ_{HB}. Experimental values of electrostatic (ionic bonding) interactions in aqueous solutions are 2-10 kcal/mol, which is the same order of magnitude as the hydrogen bonding

energy (Creighton, 1993), therefore, the maximum electrostatic interaction strength, ϵ_{CH}, is set to 1 relative to ϵ_{HB} in our study.

We explore assembly of $A\beta$16-22 peptides using the four-bead model with two different sets of interaction parameters: one with electrostatic interactions ($\epsilon_{HB} = 1$, $\epsilon_{HP} = 0.15$, and $\epsilon_{CH} = 1$) and one without electrostatic interactions ($\epsilon_{HB} = 1$, $\epsilon_{HP} = 0.15$, and $\epsilon_{CH} = 0$).

3.1 $A\beta$16-22 folding

We study the equilibrium behavior of a single peptide at different temperatures. Temperature is controlled by implementing the Berendsen thermostat method (Berendsen et al., 1984) as described in the section "Methods", subsection "Discrete molecular dynamics". At each sampled temperature, we perform 100 million simulation steps with initial random coil conformations. The heat capacity is calculated using the averages $< E >$ and $< E^2 >$ of the total potential energy E for each time frame of 10 million simulation steps, $C_v = (< E^2 > - < E >^2)/(k_B T^2)$. The average is calculated from the heat capacities of the last 6 time frames for each temperature, and the error bar shows the standard deviation of each average heat capacity.

Fig. 2 (a) shows the heat capacity as a function of temperature T for a

single $A\beta$16-22 peptide using the four-bead model with electrostatic interactions. At low temperatures, the peptide forms a loop conformation with the two termini forming a salt-bridge. This loop conformation unfolds to random coils at higher temperatures and the transition occurs over a broad temperature range centered at T=0.13. Due to the lack of explicit water molecules that can form hydrogen bonds with a peptide, we do not find the β-strand monomer conformations observed in the all-atom MD study by Klimov and Thirumalai (2003).

Fig. 2 (b) shows the heat capacity as a function of temperature T for a single $A\beta$16-22 peptide using the four-bead model with no electrostatic interactions. At low temperatures, the peptide forms an α-helical conformation. The transition from the α-helix to an unfolded state occurs at temperature 0.11. These results show that electrostatic interactions play an important role in $A\beta$16-22 folding, shifting the tendency to form an α-helical monomer conformation towards the loop-like conformation.

3.2 $A\beta$16-22 aggregation

We simulate aggregation of eight $A\beta$16-22 peptides in a cubic box of side 50Å with periodic boundary conditions at temperatures from 0.090 to 0.165

with temperature interval of 0.005. In the four-bead model with electrostatic interactions, we acquire 2 trajectories of 12M simulation steps at each temperature. To investigate the effect of electrostatic interactions (Klimov and Thirumalai, 2003; Favrin et al., 2004), we acquire one trajectory of 20 million simulation steps at each temperature in the four-bead model with no electrostatic interactions. Different trajectories have different initial conformation, in which monomer peptides are separated and in random coil conformations.

We first simulate aggregation of 8 peptides in the four-bead model with electrostatic interactions. At temperatures between 0.130 and 0.145, all peptides initially collapse into an amorphous structure due to favorable desolvation energetics of the hydrophobic side-chain atoms, then hydrogen bonds form one-by-one followed by conformational rearrangements of the peptides, leading to the formation of ordered two-layer antiparallel β-sheets. Edge strands are free to further form hydrogen bonds, suggesting that the β-sheet aggregate may be a building block of fibril formation. Fig. 3 (top) shows the time evolution of $A\beta$16-22 aggregation at temperature of 0.130.

We further simulate aggregation of 8 peptides in the four-bead model without electrostatic interactions. The peptides only aggregate into amorphous structures. Fig. 3 (bottom) shows the time evolution of the aggregation

of the peptides at temperature of 0.130. Our results show that the electrostatic interactions are critical for the ordered antiparallel structure of the aggregate in agreement with Klimov and Thirumalai (2003).

To check whether more β-sheets can be formed with a larger number of peptides, we also study the aggregation of 16 $A\beta$16-22 peptides. In the model with electrostatic interactions, a three-layer β-sheet structure is formed (Fig. 4). In the model without electrostatic interactions, peptides only form amorphous structures. Fig. 5 (a,b) shows two typical amorphous structures at two different temperatures. At a lower T=0.110 we see hydrogen bonds forming inside the aggregate.

Time evolution of $A\beta$16-22 aggregation suggests that in the model with electrostatic interactions the aggregation process consists of two stages – the initial globular hydrophobic collapse and the later hydrogen bond formation leading to an ordered β-sheet structure. Thus, we study melting of this ordered anti-parallel $A\beta$16-22 structure. We use as a starting conformation the three-layer β-sheet structure of 16 $A\beta$16-22 peptides and perform simulations at a wide range of temperatures. At each temperature we perform 10 million simulation steps. It takes less than 10^5 simulation steps to reach equilibrium at each temperature.

Fig. 6 (a) shows the temperature dependence of the heat capacity and the average number of hydrogen bonds as defined within the four-bead model. The two peaks in the heat capacity indicate a two-stage melting process. The first peak corresponds to the melting (dissociation) of hydrogen bonds, and the second one to the melting of hydrophobic contacts. In the model with no electrostatic interactions, peptides only aggregate into amorphous structures at all temperatures. Fig. 6 (b) shows the temperature dependence of the heat capacity and the average number of hydrogen bonds. At low temperatures such as 0.050, the average numbers of hydrogen bonds for the two cases (with and without electrostatic interactions) are almost the same. This is due to a loose definition of the hydrogen bond in the four-bead model (angular restriction is not that strict due to absence of the oxygen atom). The difference in hydrogen bonds between Fig. 6(a) and Fig. 6(b) is that in Fig. 6(a) hydrogen bonds are ordered, while in Fig. 6(b) their orientation is uniformly distributed in three-dimensions.

Fig. 7 shows the comparison of temperature dependence of the total potential energy and potential energy contributions from three different types of interactions (hydrogen bond, hydropathic, and electrostatic interaction) for the system of 16 $A\beta$16-22 peptides in the model with and without electro-

static interactions. For an individual conformation, potential energy contribution from hydrophobic (electrostatic) interactions is the summation of all the potential energies from the hydrophobic (electrostatic) interaction pairs based on the distance dependence of the hydrophobic interaction potentials in Fig 1 (a) (the electrostatic interaction potential function in Fig 1 (b)). Conformations are recorded every 10^4 simulation steps. The last 600 conformations at each temperature are used for the calculation of the average potential energy contributions. The energy contributions due to hydrogen bonds are calculated by subtracting other contributions from the total potential energy. The energy contribution due to hydrophobic interactions is the most important. In the model with electrostatic interactions, the energy contribution due to hydrogen bond interactions is comparible to the one of electrostatic interactions.

Fig. 8 shows the setup of the diffraction pattern computation and the calculated diffraction pattern (Ding et al., 2002b; Peng et al., 2004). The fibril axis is along the y-axis. The relatively sharp and intense 4.8 Å meridional reflections correspond to the periodic packing of β-strands along the fibril axis and the weaker equatorial reflections correspond to the distance between β-sheets. The distance between β-sheets is 10–11Å according to

experiments, but in our simulations this distance is around 6.4Å. This is due to an underestimated size of the side-chains in our model. If we shift the interaction range between side-chains from [3.07Å, 7.5 Å] to [4.0Å, 8.5Å] to mimic the effect of larger side-chains, we find that the peptides still aggregate into three-layer β-sheets. The computed diffraction pattern shows that the distance between β-strands within a sheet remains the same (4.8Å), but the distance between β-sheets increases to 7.5Å. These simulations show that in order to achieve a quantitative agreement with experimental results, more detailed interaction ranges need to be implemented in the model. A similar difference between inter-sheet distances determined *in silico* and *in vitro* has been reported by Nguyen and Hall (2004a), who also used the four-bead peptide model.

4 Discussion and Conclusion

DMD simulations with the four-bead peptide model enable us to visualize the process of $A\beta$16-22 aggregation from randomly-oriented monomer peptides to structured, fibril-like subunits. These subunits consist of stacked β-sheets, a result consistent with the common cross-β core structures determined for

amyloid fibrils in X-ray diffraction studies (Eanes and Glenner, 1968; Sunde et al., 1997) and previous simulation work (Ma and Nussinov, 2002; Klimov and Thirumalai, 2003; Favrin et al., 2004; Santini et al., 2004a). Within each β-sheet, the peptides are in an antiparallel arrangement, which is consistent with solid-state NMR results for $A\beta$16-22 fibrils at pH 7.4 (Balbach et al., 2000; Tycko and Ishii, 2003; Petkova et al., 2004).

The simulations without electrostatic interactions show that peptides only aggregate into amorphous structures. This suggests that the electrostatic interactions are essential for the ordered antiparallel arrangement, as suggested by Klimov and Thirumalai (2003). This conclusion is not consistent with the Monte Carlo simulation results by Favrin et al. (2004) stating that $A\beta$16-22 prefers antiparallel β-strand orientation even in the absence of electrostatic interactions.

The aggregation process involves two stages – the initial globular hydrophobic collapse and the later hydrogen bond formation. In the investigation of the stability of the layered β-sheets, we find that the melting of the β-sheets shows also the two-stage feature: first hydrogen bonds' melting leads to the amorphous (disordered) structures, and then the loss of hydrophobic contacts leads to the disaggregation. Differential scanning calorimetry has

been used to investigate the thermal transitions of type I collagen fibrils and the melting curves display two pronounced heat adsorption peaks (Tiktopulo and Kajava, 1998). This method could also be applied to study the melting of amyloid fibrils. This two-stage process might reflect a similar behavior of a full-length $A\beta$, which first forms unstructured, amorphous oligomers, which later, through further assembly, yield protofibrils, rich in hydrogen-bonded β-strand structure (Bitan et al., 2003; Klein et al., 2004).

We thank the Memory Ride Foundation for support, F. Ding and N. V. Dokholyan for the implementation of the four-bead protein model, and G. Bitan, N. Lazo, and S. Maji for helpful discussions. This work was supported in part by NIH grants NS38328, NS44147, and AG18921 to D.B. Teplow.

References

Alzheimer, A. 1906. über einen eigenartigen schweren erkrankungsprozeß der hirnrinde. *Neurologisches Centralblatt.* 23:1129–1136.

Balbach, J. J., Y. Ishii, O. N. Antzutkin, R. D. Leapman, N. W. Rizzo, F. Dyda, J. Reed, and R. Tycko. 2000. Amyloid fibril formation by $A\beta_{16-22}$,

a seven-residue fragment of the Alzheimer's β-amyloid peptide, and structural characterization by solid state NMR. *Biochemistry.* 39:13748–13759.

Berendsen, H. J. C., J. Poastma, W. V. Gunsteren, A. DiNola, and J. Haak. 1984. Molecular dynamics with coupling to an external bath. *J. Chem. Phys.* 81:3684–3690.

Bitan, G., M. D. Kirkitadze, A. Lomakin, S. S. Vollers, G. B. Benedek, and D. B. Teplow. 2003. Amyloid β-protein (Aβ) assembly: Aβ40 and Aβ42 oligomerize through distinct pathways. *Proc. Natl. Acad. Sci. USA.* 100:330–335.

Borreguero, J. M., N. V. Dokholyan, S. V. Buldyrev, E. I. Shakhnovich, and H. E. Stanley. 2002. Thermodynamics and folding kinetics analysis of the SH3 domain from discrete molecular dynamics. *J. Mol. Biol.* 318:863–876.

Borreguero, J. M., B. Urbanc, N. D. Lazo, S. V. Buldyrev, D. B. Teplow, and H. E. Stanley. 2005. Folding events in the 21-30 region of amyloid β-protein (Aβ) studied *in silico*. *Proc. Natl. Acad. Sci. USA*. 102:6015–6020.

Creighton, T. 1993. Proteins: structures and molecular properties, second edition. W. H. Freeman and Co., New York.

Ding, F., J. M. Borreguero, S. V. Buldyrey, H. E. Stanley, and N. V. Dokholyan. 2003. Mechanism for the α-helix to β-hairpin transition. *Proteins: Struct. Func. & Genet.* 53:220–228.

Ding, F., S. V. Buldyrev, and N. V. Dokholyan. 2005. Folding Trp-cage to NMR resolution native structure using a coarse-grained model. *Biophys. J.* 88:147–155.

Ding, F., N. V. Dokholyan, S. V. Buldyrev, H. E. Stanley, and E. I. Shakhnovich. 2002a. Direct molecular dynamics observation of protein folding transition state ensemble. *Biophys. J.* 83:3525–3532.

Ding, F., N. V. Dokholyan, S. V. Buldyrev, H. E. Stanley, and E. I. Shakhnovich. 2002b. Molecular dynamics simulation of the SH3 domain aggregation suggests a generic amyloidogenesis mechanism. *J. Mol. Biol.* 324:851–857.

Dokholyan, N. V., S. V. Buldyrev, H. E. Stanley, and E. I. Shakhnovich. 1998. Discrete molecular dynamics studies of the folding of a protein-like model. *Fold. Des.* 3:577–587.

Eanes, E. D., and G. G. Glenner. 1968. X-ray diffraction studies on amyloid filaments. *J. Histochem. Cytochem.* 16:673–677.

Esler, W. P., E. R. Stimson, J. R. Ghilardi, Y. A. Lu, A. M. Felix, H. V. Vinters, P. W. Mantyh, J. P. Lee, and J. E. Maggio. 1996. Point substitution in the central hydrophobic cluster of a human β-amyloid congener disrupts peptide folding and abolishes plaque competence. *Biochemistry.* 35:13914–21.

Favrin, G., A. Irbäck, and S. Mohanty. 2004. Oligomerization of amyloid Aβ16-22 peptides using hydrogen bonds and hydrophobicity forces. *Biophys. J.* 87:3657–3664.

Gsponer, J., U. Haberthür, and A. Caflisch. 2003. The role of side-chain interactions in the early steps of aggregation: Molecular dynamics simulations of an amyloid-forming peptide from the yeast prion Sup35. *Proc. Natl. Acad. Sci. USA.* 100:5154–9.

Hardy, J., and D. J. Selkoe. 2002. The amyloid hypothesis of Alzheimer's disease: Progress and problems on the road to therapeutics. *Science.* 297:353–356.

Humphrey, W., A. Dalke, and K. Schulten. 1996. VMD: visual molecular dynamics. *J. Mol. Graph.* 14:33–38.

Hwang, W., S. Zhang, R. D. Kamm, and M. Karplus. 2004. Kinetic control

of dimer structure formation in amyloid fibrillogenesis. *Proc. Natl. Acad. Sci. USA.* 101:12916–12921.

Kirkitadze, M. D., G. Bitan, and D. B. Teplow. 2002. Paradigm shifts in Alzheimer's disease and other neurodegenerative disorders: the emerging role of oligomeric assemblies. *J. Neurosci. Res.* 69:567–577.

Klein, W. L., G. A. Krafft, and C. E. Finch. 2001. Targeting small $A\beta$ oligomers: the solution to an Alzheimer's disease conundrum? *Trends Neurosci.* 24:219–224.

Klein, W. L., W. B. Stine, and D. B. Teplow. 2004. Small assemblies of unmodified amyloid β-protein are the proximate neurotoxin in Alzheimer's disease. *Neurobiol. Aging.* 25:569–580.

Klimov, D. K., J. E. Straub, and D. Thirumalai. 2004. Aqueous urea solution destabilizes Aβ(16-22) oligomers. *Proc. Natl. Acad. Sci. USA.* 101:14760–14765.

Klimov, D. K., and D. Thirumalai. 2003. Dissecting the assembly of $A\beta_{16-22}$ amyloid peptides into antiparallel β sheets. *Structure.* 11:295–307.

Kyte, J., and R. F. Doolittle. 1982. A simple method for displaying the hydropathic character of a protein. *J. Mol. Biol.* 157:105–132.

Lambert, M. P., A. K. Barlow, B. A. Chromy, C. Edwards, R. Freed, M. Liosatos, T. E. Morgan, I. Rozovsky, B. Trommer, K. L. Viola, P. Wals, C. Zhang, C. E. Finch, G. A. Krafft, and W. L. Klein. 1998. Diffusible, nonfibrillar ligands derived from $A\beta_{1-42}$ are potent central nervous system neurotoxins. *Proc. Natl. Acad. Sci. USA.* 95:6448–6453.

Lynn, D. G., and S. C. Meredith. 2000. Review: model peptides and the physicochemical approach to β-amyloids. *J. Struct. Biol.* 130:153–173.

Ma, B., and R. Nussinov. 2002. Stabilities and conformations of Alzheimer's β-amyloid peptide oligomers ($A\beta_{16-22}$, $A\beta_{16-35}$, and $A\beta_{10-35}$): sequence effects. *Proc. Natl. Acad. Sci. USA.* 99:14126–14131.

Malinchik, S. B., H. Inouye, K. E. Szumowski, and D. A. Kirschner. 1998. Structural analysis of Alzheimer's β(1-40) amyloid: protofilament assembly of tubular fibrils. *Biophys. J.* 74:537–545.

Nguyen, H. D., and C. K. Hall. 2004a. Molecular dynamics simulations of spontaneous fibril formation by random-coil peptides. *Proc. Natl. Acad. Sci. USA.* 101:16180–16185.

Nguyen, H. D., and C. K. Hall. 2004b. Phase diagrams describing fibrillization by polyalanine peptides. *Biophys. J.* 87:4122–4134.

Nguyen, H. D., and C. K. Hall. 2005. Kinetics of fibril formation by polyalanine peptides. *J. Biol. Chem.* 280:9074–9082.

Paci, E., J. Gsponer, X. Salvatella, and M. Vendruscolo. 2004. Molecular dynamics studies of the process of amyloid aggregation of peptide fragments of transthyretin. *J. Mol. Biol.* 340:555–69.

Peng, S., F. Ding, B. Urbanc, S. V. Buldyrev, L. Cruz, H. E. Stanley, and N. V. Dokholyan. 2004. Discrete molecular dynamics simulations of peptide aggregation. *Phys. Rev. E.* 69:041908.

Petkova, A. T., G. Buntkowsky, F. Dyda, R. D. Leapman, W.-M. Yau, and R. Tycko. 2004. Solid state NMR reveals a pH-dependent antiparallel β-sheet registry in fibrils formed by a β-amyloid peptide. *J. Mol. Biol.* 335:247–260.

Rapaport, D. C. 1997. The art of molecular dynamics simulation. Cambridge University Press, Cambridge.

Richardson, J. S., and D. C. Richardson. 2002. Natural β-sheet proteins use

negative design to avoid edge-to-edge aggregation. *Proc. Natl. Acad. Sci. USA*. 99:2754–2759.

Roher, A. E., J. Baudry, M. O. Chaney, Y. M. Kuo, W. B. Stine, and M. R. Emmerling. 2000. Oligomerizaiton and fibril asssembly of the amyloid-β protein. *Biochim. Biophys. Acta.* 1502:31–43.

Rottkamp, C. A., C. S. Atwood, J. A. Joseph, A. Nunomura, G. Perry, and M. A. Smith. 2002. The state versus amyloid-β: the trial of the most wanted criminal in Alzheimer disease. *Peptides.* 23:1333–1341.

Santini, S., N. Mousseau, and P. Derreumaux. 2004a. In silico assembly of Alzheimer's Aβ16-22 peptide into β-sheets. *J. Am. Chem. Soc.* 126:11509–11516.

Santini, S., G. Wei, N. Mousseau, and P. Derreumaux. 2004b. Pathway complexity of Alzheimer's β-amyloid Aβ16-22 peptide assembly. *Structure.* 12:1245–1255.

Selkoe, D. J. 1991. The molecular pathology of Alzheimer's disease. *Neuron.* 6:487–498.

Selkoe, D. J. 2001. Alzheimer's disease: Genes, proteins, and therapy. *Physiol. Rev.* 81:741–766.

Serpell, L. C. 2000. Alzheimer's amyloid fibrils: structure and assembly. *Biochim. Biophys. Acta.* 1502:16–30.

Shakhnovich, E. I. 1996. Modeling protein folding: the beauty and power of simplicity. *Fold. Des.* 1:R50–R54.

Smith, A. V., and C. K. Hall. 2001a. Assembly of a tetrameric α-helical bundle: computer simulations on an intermediate-resolution protein model. *Proteins: Struct. Func. & Genet.* 44:376–391.

Smith, A. V., and C. K. Hall. 2001b. Protein refolding versus aggregation: Computer simulations on an intermediate-resolution protein model. *J. Mol. Biol.* 312:187–202.

Sunde, M., L. C. Serpell, M. Bartlam, P. E. Fraser, M. B. Pepys, and C. C. Blake. 1997. Common core structure of amyloid fibrils by synchrotron X-ray diffraction. *J. Mol. Biol.* 273:729–739.

Takada, S., Z. Luthey-Schulten, and P. G. Wolynes. 1999. Folding dynamics

with nonadditive forces: A simulation study of a designed helical protein and a random heteropolymer. *J. Chem. Phys.* 110:11616–11629.

Taylor, J. P., J. Hardy, and K. H. Fischbeck. 2002. Toxic proteins in neurodegenerative disease. *Science.* 296:1991–1995.

Tiktopulo, E. I., and A. V. Kajava. 1998. Denaturation of type I collagen fibrils is an endothermic process accompanied by a noticeable change in the partial heat capacity. *Biochemistry.* 37:8147–52.

Tycko, R., and Y. Ishii. 2003. Constraints on supramolecular structure in amyloid fibrils from two-dimensional solid-state NMR spectroscopy with uniform isotopic labeling. *J. Am. Chem. Soc.* 125:6606–6607.

Urbanc, B., L. Cruz, F. Ding, D. Sammond, S. Khare, S. V. Buldyrev, H. E. Stanley, and N. V. Dokholyan. 2004a. Molecular dynamics simulation of amyloid β dimer formation. *Biophys. J.* 87:2310–2321.

Urbanc, B., L. Cruz, S. Yun, S. V. Buldyrev, G. Bitan, D. B. Teplow, and H. E. Stanley. 2004b. *In silico* study of amyloid β-protein folding and oligomerization. *Proc. Natl. Acad. Sci. USA.* 101:17345–17350.

Walsh, D. M., D. M. Hartley, Y. Kusumoto, Y. Fezoui, M. M. Condron,

A. Lomakin, G. B. Benedek, D. J. Selkoe, and D. B. Teplow. 1999. Amyloid β-protein fibrillogenesis. Structure and biological activity of protofibrillar intermediates. *J. Biol. Chem.* 274:25945–25952.

Wei, G., N. Mousseau, and P. Derreumaux. 2004. Sampling the self-assembly pathways of KFFE hexamers. *Biophys. J.* 87:3648–56.

Xiong, H., B. L. Buckwalter, H. M. Shieh, and M. H. Hecht. 1995. Periodicity of polar and nonpolar amino acids is the major determinant of secondary structure in self-assembling oligomeric peptides. *Proc. Natl. Acad. Sci. USA.* 92:6349–53.

Zhou, Y. Q., and M. Karplus. 1997. Folding thermodynamics of a model three-helix-bundle protein. *Proc. Natl. Acad. Sci. USA.* 94:14429–14432.

Zhou, Y. Q., and M. Karplus. 1999. Folding of a model three-helix bundle protein: A thermodynamic and kinetic analysis. *J. Mol. Biol.* 293:917–951.

Figure captions:

Figure 1: The amino acid-specific interactions between side-chain atoms. (a) Effective hydrophobic attraction (solid line) between two hydrophobic side-chains and effective hydrophilic repulsion (dashed line) between two hydrophilic side-chains. (b) The electrostatic interactions. Attraction (solid line) between two oppositely-charged side-chains and repulsion (dashed line) between two identically-charged side-chains. The hard-core repulsion distance is 3.07Å and the distance above which there is no interaction is 7.5Å.

Figure 2: Temperature dependence of heat capacities for a single $A\beta$16-22 peptide (a) with and (b) without electrostatic interactions. The insets show folded conformations of a single $A\beta$16-22 peptide as predicted by our four-bead model at low temperatures. The conformations are visualized using the program *VMD* (Humphrey et al., 1996).

Figure 3: Time evolution of aggregation of eight $A\beta$16-22 peptides at a temperature of 0.130 in the four-bead model with (top) and without (bottom) electrostatic interactions. (a) Initially, all peptides are in random coil

conformations and are randomly placed within a simulation box. (b) and (c) Intermediate structures after 0.2 and 2 million simulation steps, respectively. (d) After 12 million simulation steps. Peptides aggregate into a two-layer β-sheet structure in the model with electrostatic interactions while they aggregate into an amorphous structure in the absence of electrostatic interactions. The conformations are visualized with the program *VMD* (Humphrey et al., 1996).

Figure 4: Ordered antiparallel β-sheet structure of 16 $A\beta$16-22 peptides obtained in the model with electrostatic interactions at a temperature of 0.155 after 4M simulation steps. (a) and (b) are side and top views, respectively. The fibril axis is denoted as the y-axis.

Figure 5: Amorphous structure of 16 $A\beta$16-22 peptides obtained in the model without electrostatic interaction at temperatures (a) T=0.110 and (b) T=0.150 after 20 million simulation steps. The conformations are visualized using the program *VMD* (Humphrey et al., 1996).

Figure 6: (a) Temperature dependence of the heat capacity and the aver-

age number of hydrogen bonds of 16 $A\beta$16-22 peptides in the four-bead model with electrostatic interactions. (b) Temperature dependence of the heat capacity and the average number of hydrogen bonds of 16 $A\beta$16-22 peptides in the four-bead model without electrostatic interactions. The insets show the hydrogen bond orientations in the modle with electrostatic interactions (a) and in the model without electrostatic interactions (b). Insets are created using the program *VMD* (Humphrey et al., 1996).

Figure 7: Temperature dependence of the total potential energy and the potential energy contributions from three different types of interactions: hydrogen bond, hydropathic, and electrostatic interaction for the system of 16 $A\beta$16-22 peptides in the model (a) with interaction interactions and (b) without electrostatic interactions.

Figure 8: (a) Setup of a diffraction pattern calculation for the three-layer β-sheet aggregate formed by 16 $A\beta$16-22 peptides. The fibril axis is along the y-axis and the scattering occurs along the z-axis, which is perpendicular to the plane of the figure. (b) Averaged computed diffraction intensity that would appear on the x-y plane behind the aggregate. The averaged intensity

is obtained by averaging over 20 intensities obtained by successive rotations of the aggregate around the y-axis by 18^o. The stronger intensity peaks at 4.8Å along the y-axis correspond to the distance between the neighboring β-strands within a β-sheet, and the dimmer intensity peaks at 6.4Å correspond to the distance between the neighboring β-sheets.

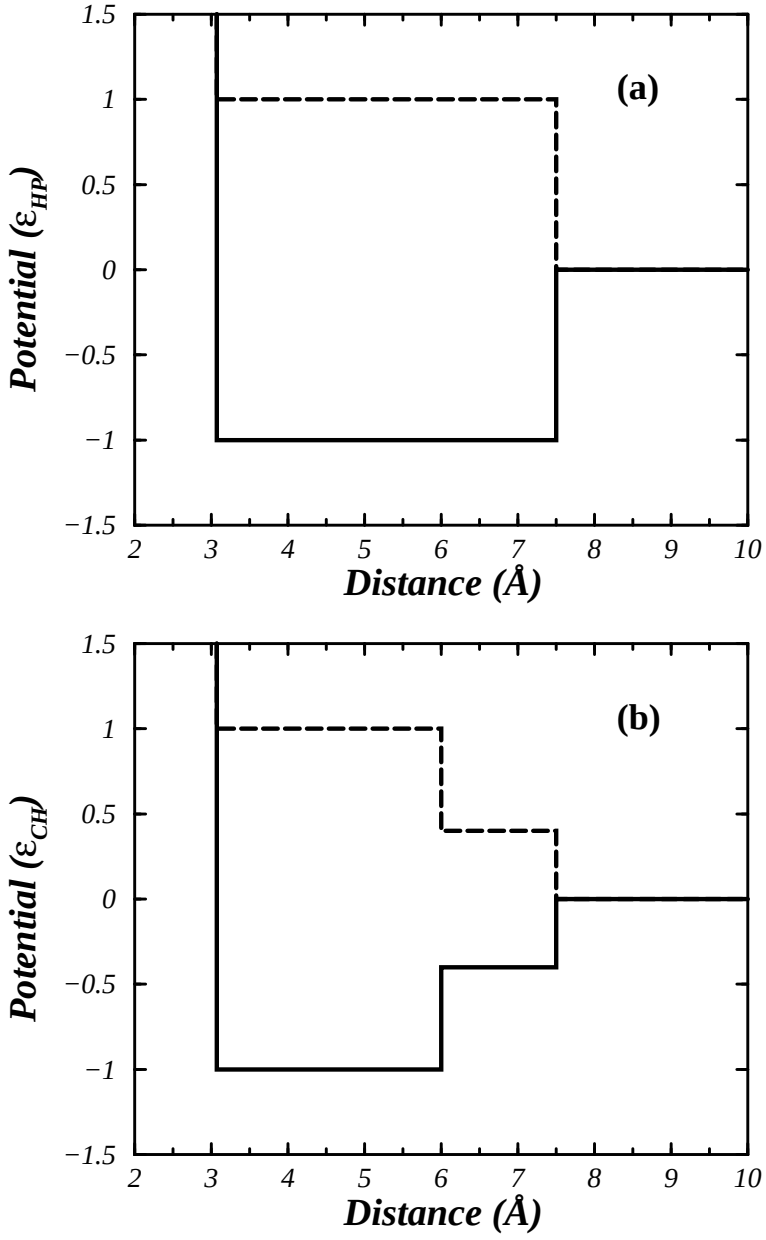
(a)
Potential (ε_{HP})
Distance (Å)
(b)
Potential (ε_{CH})
Distance (Å)

Figure 1:

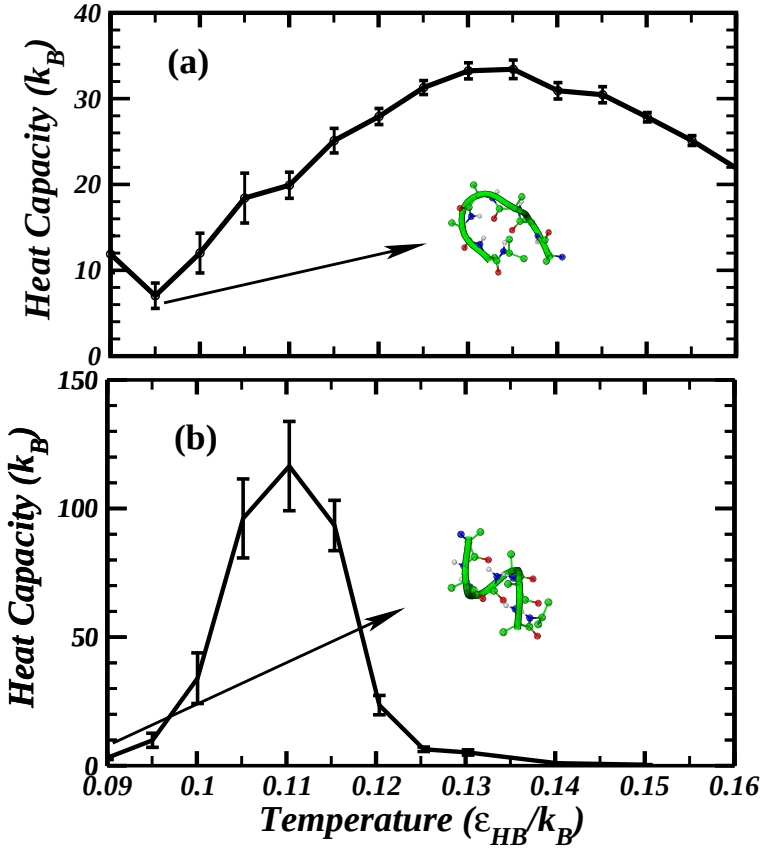
(a)
(b)
Heat Capacity (k_B)
Heat Capacity (k_B)
Temperature (ε_{HB}/k_B)
0
10
20
30
40
0
50
100
150
0.09
0.1
0.11
0.12
0.13
0.14
0.15
0.16

Figure 2:

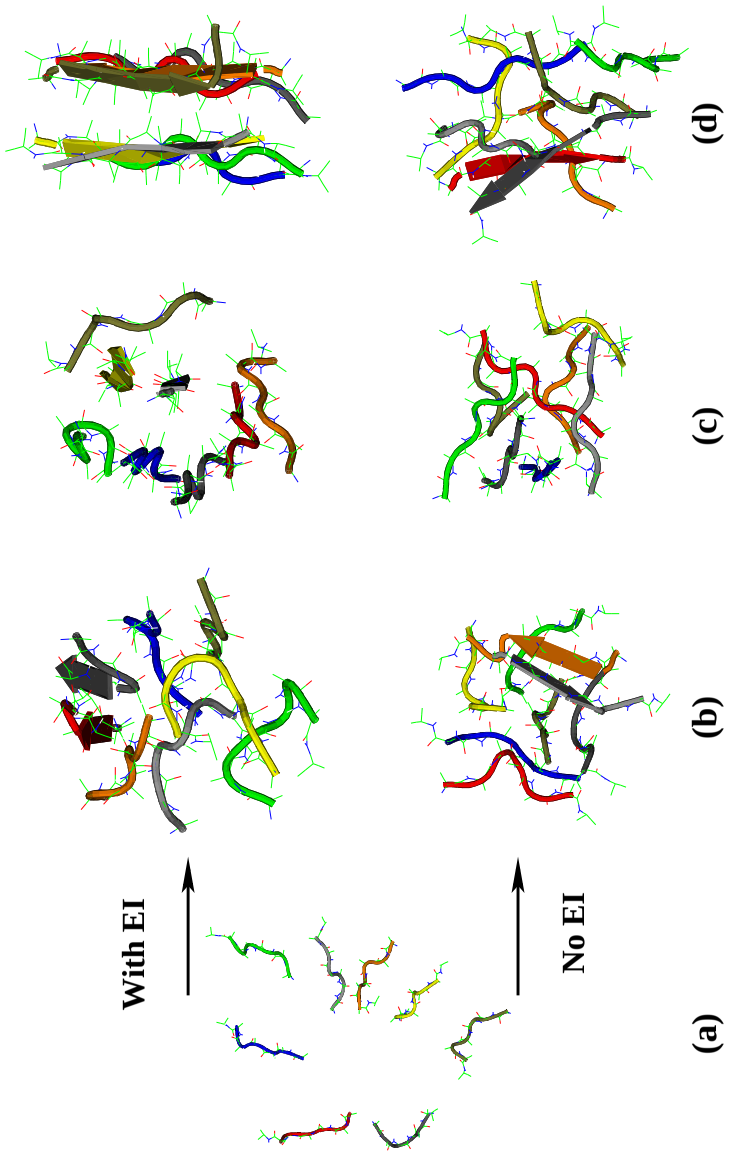

Figure 3:

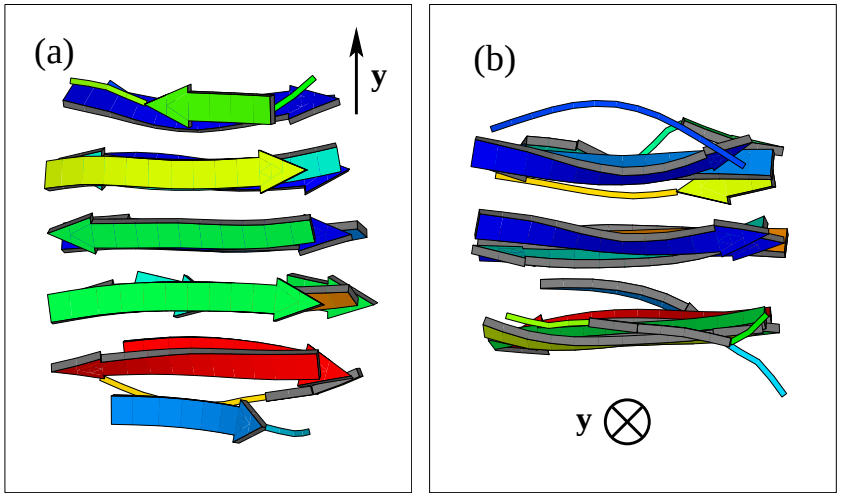

Figure 4:

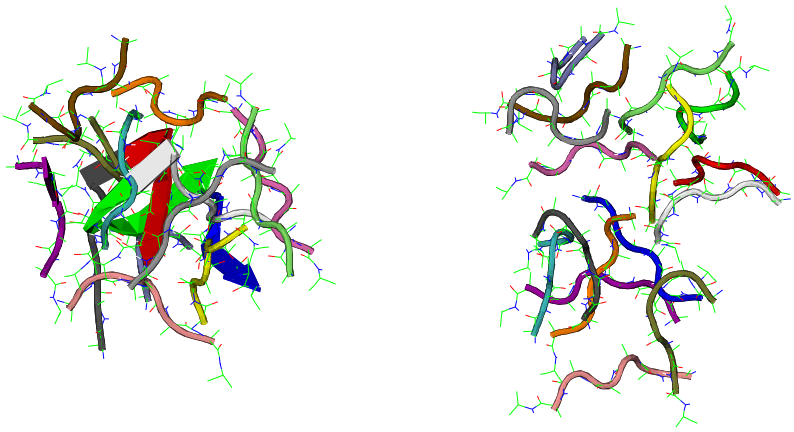

(a) T=0.110 (b) T=0.150

Figure 5:

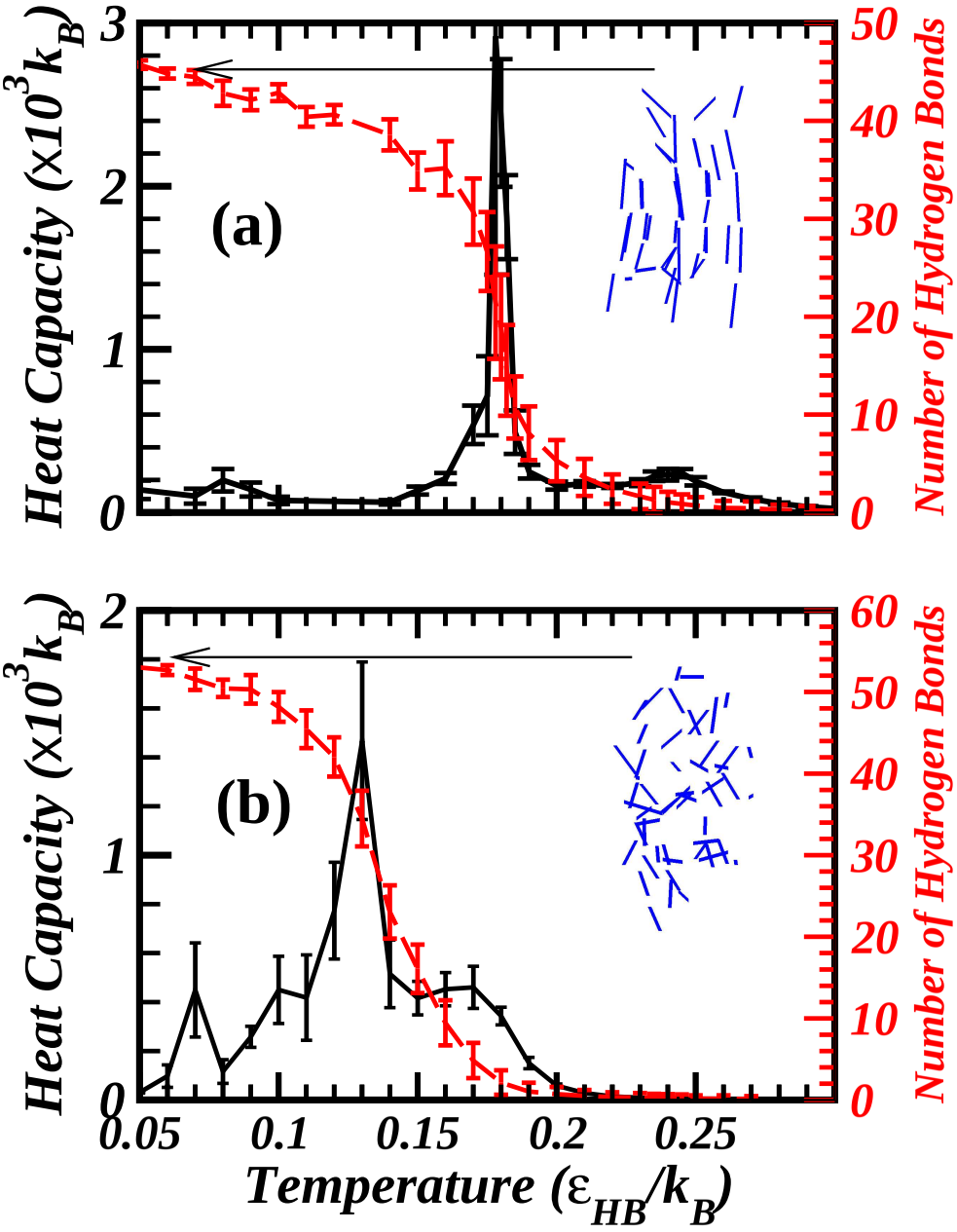
(a)
(b)
Heat Capacity (x10^3 k_B)
Number of Hydrogen Bonds
Temperature (ε_HB/k_B)
0
1
2
3
0.05
0.1
0.15
0.2
0.25
10
20
30
40
50
60

Figure 6:

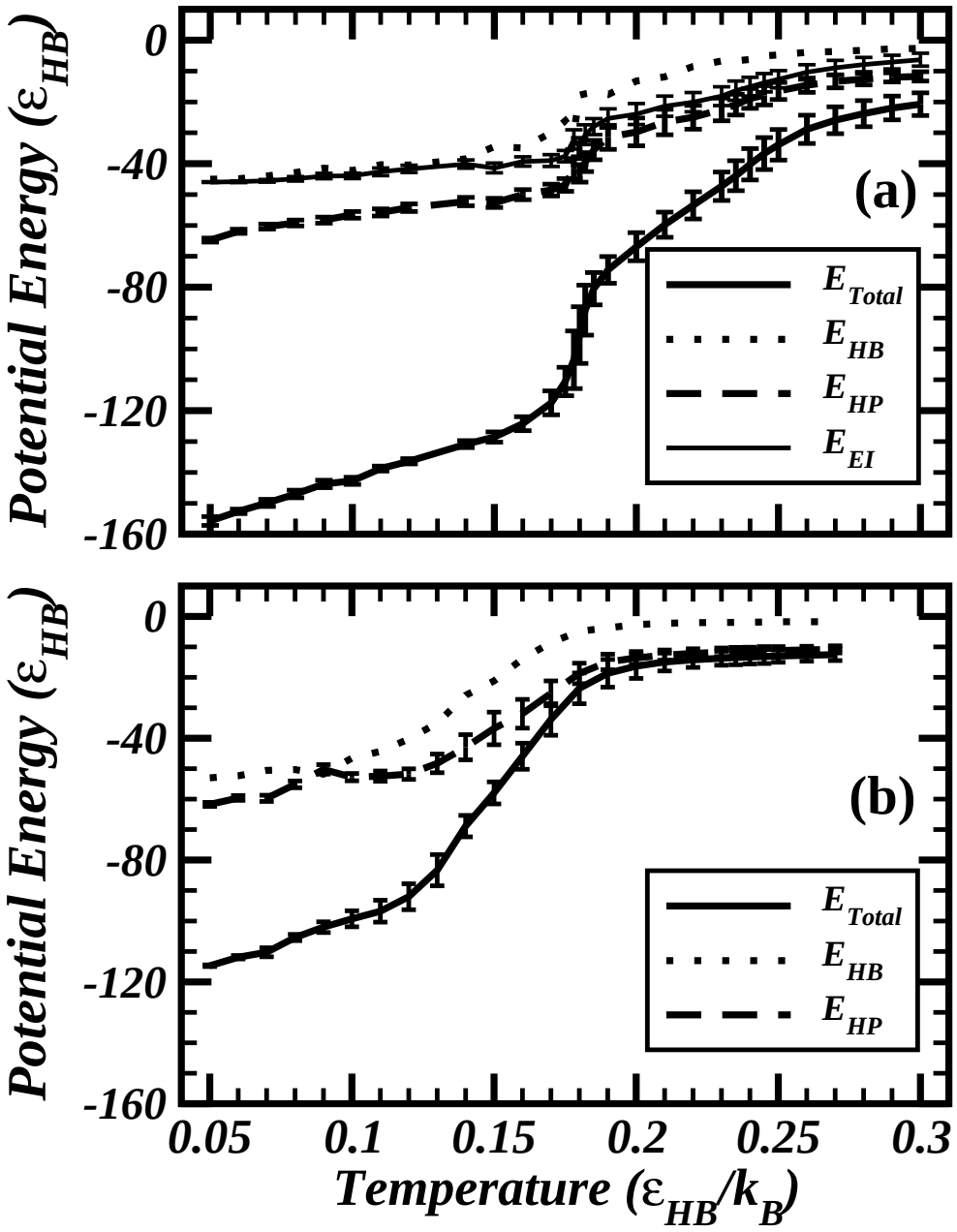
Potential Energy (ε_{HB})
0
-40
-80
-120
-160
(a)
E_{Total}
E_{HB}
E_{HP}
E_{EI}
Potential Energy (ε_{HB})
0
-40
-80
-120
-160
(b)
E_{Total}
E_{HB}
E_{HP}
0.05
0.1
0.15
0.2
0.25
0.3
Temperature (ε_{HB}/k_B)

Figure 7:

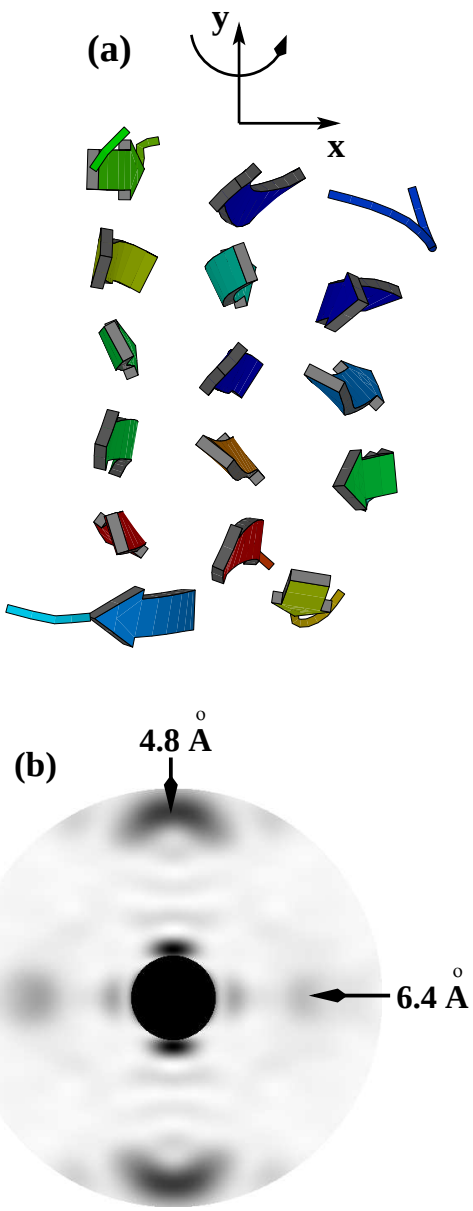

Figure 8: